Higher Order PN Solver in Method of Characteristics Code STREAM

Anisur Rahman, Alexey Cherezov, and Deokjung Lee
Department of Nuclear Engineering, Ulsan National Institute of Science and Technology
50 UNIST-gil, Ulsan, 44919, Republic of Korea
**Corresponding author: anisur@unist.ac.kr, deokjung@unist.ac.kr*

1. Introduction

STREAM [1], A three-dimensional method of characteristics (MOC) neutron transport code for light water nuclear reactor core analysis. Now a day direct 3D neutron transport model is popular for nuclear reactor analysis because of without approximation, availability of computer capability and more accurate results. General task of transport model is to solve time, energy and space dependent the Boltzmann neutron transport equation. In MOC, rewrite the multi-dimensional partial differential equation to an ordinary differential equation along a characteristic curve. Flat, Linear and Quadratic neutron source approximation used in MOC, nevertheless flat neutron source is more popular compare to others because of simplicity although Linear and Quadratic neutron source approximation allow bigger mesh to compare flat source. Flat source approximation with the used of higher order angle dependent neutron flux could generate more realistic outcome. In higher order, the scattering source is based on spherical harmonics (PN method) with Legendre polynomial functions. The scattering source is expanded using spherical harmonics odd and even parity of source components. Finally, the angular and scalar flux are calculated from the sources.

MOC is widely used in two-dimensional neutron transport reactor physics field. On the other hand, flux and source are expressed with the combination of 2D radial and 1D axial component in 3D MOC problem. The flat source approximation with higher order scattering source scheme is capable to improve the solution accuracy in both isotropic and anisotropic sources with respect to the reference solution. This paper demonstrates up to order 3.

STREAM uses 72-group library which was generated from continuous energy and 8-group is used for the CMFD. Convergence criteria for both k-effective and fission source use as STREAM default values (1.0E-5).

2. Methodology

2.1 3D Method of Characteristics

The 3D neutron transport equation in method of characteristics is a combination of 2D radial (x, y) and 1D axial component. The 3D angular flux, scalar flux and source are written with radial and axial parts as:

$$\begin{aligned}\psi^g_{i,j,k}(s,z) &\approx \psi^g_{i,j,k}(s)b(z)\\ \phi^g(s,z) &\approx \bar{\phi}^g_m b(z)\\ Q^g_{i,j}(s,z) &\approx \bar{Q}^g_{i,j,m}b(z)\end{aligned} \quad (1)$$

where s is the radial coordinate in the x-y plane; z is the coordinate in the axial direction; i is the index of azimuthal angle; j is the index of polar angle; k is the index for MOC ray segment; g is the index of energy group; and m is the index for source region.

For the axial domain (plane), the component of angular flux, scalar flux and source are written with a linear combination of upper and lower domain. Thus:

$$\begin{cases}\psi^g_{i,j,k}(s)b(z) = \psi^{g,0}_{i,j,k}(s) + \frac{z}{\Delta z}(\psi^{g,+}_{i,j,k}(s) - \psi^{g,-}_{i,j,k}(s))\\ \bar{\phi}^g_m b(z) = \bar{\phi}^{g,0}_m + \frac{z}{\Delta z}(\bar{\phi}^{g,+}_m - \bar{\phi}^{g,-}_m) \qquad \frac{-\Delta z}{2} \le z \le \frac{\Delta z}{2}\\ \bar{Q}^g_{i,j,m}b(z) = \bar{Q}^{g,0}_{i,j,m} + \frac{z}{\Delta z}(\bar{Q}^{g,+}_{i,j,m} - \bar{Q}^{g,-}_{i,j,m})\end{cases} (2)$$

where z^0, z^+ and z^- are active, upper and lower region of the axial plane. The axial-average of each value is defined as:

$$\begin{cases}\psi^{g,0}_{i,j,k}(s) = \frac{1}{2}(\psi^{g,+}_{i,j,k}(s) + \psi^{g,-}_{i,j,k}(s))\\ \bar{\phi}^{g,0}_m = \frac{1}{2}(\bar{\phi}^{g,+}_m + \bar{\phi}^{g,-}_m)\\ \bar{Q}^{g,0}_{i,j,m} = \frac{1}{2}(\bar{Q}^{g,+}_{i,j,m} + \bar{Q}^{g,-}_{i,j,m})\end{cases} (3)$$

The steady-state 3D neutron transport equation [1] along the characteristic line is

$$\cos\bar{\theta}_j \frac{\partial \psi^g_{i,j,k}(s,z)}{\partial s} + \sin\bar{\theta}_j \frac{\partial \psi^g_{i,j,k}(s,z)}{\partial z} + \Sigma^g_{tr,m}\psi^g_{i,j,k}(s,z) = Q^g_{i,j,m}(s,z) \quad (4)$$

where $\Sigma^g_{tr,m}$ is the transport cross section (XS) at flat source region m.

Inserting the approximation of flux and source from Eq. (1) to (3) into Eq. (4), the transport equation is

$$\cos\bar{\theta}_j \frac{\partial \psi^g_{i,j,k}(s)b(z)}{\partial s} + \sin\bar{\theta}_j \frac{\partial \psi^g_{i,j,k}(s)b(z)}{\partial z} + \Sigma^g_{tr,m}\psi^g_{i,j,k}(s)b(z) = \bar{Q}^g_{i,j,m}b(z) \quad (5)$$

Integrating Eq. (5) over the axial domain and dividing by size of domain:

$$\cos\bar{\theta}_j \frac{\partial \psi^{g,0}_{i,j,k}(s)}{\partial s} + \frac{\sin\bar{\theta}_j}{\Delta z}\left(\psi^{g,+}_{i,j,k}(s) - \psi^{g,-}_{i,j,k}(s)\right) + \Sigma^g_{tr,m}\psi^{g,0}_{i,j,k}(s) = \bar{Q}^{g,0}_{i,j,m} \quad (6)$$

where the source is sum of the fission and scattering source defined as follow:

$$\bar{Q}^{g,0}_{i,j,m} = \frac{1}{4\pi}\left(\frac{\chi^g_m}{k_{eff}}\sum_{g'}\nu\Sigma^{g'}_{f,m}\bar{\phi}^{g',0}_m + \sum_{g'}\Sigma^{g'\to g}_{s,m}\bar{\phi}^{g',0}_m\right) \quad (7)$$

Rewrite Eq. (6) by adding the term $\frac{2\sin\bar{\theta}_j}{\Delta z}\psi^{g,-}_{i,j,k}(s)$ in both side

$$\cos\bar{\theta}_j \frac{\partial \psi^{g,0}_{i,j,k}(s)}{\partial s} + \frac{2\sin\bar{\theta}_j}{\Delta z}\psi^{g,0}_{i,j,k}(s) + \Sigma^g_{tr,m}\psi^{g,0}_{i,j,k}(s) = \bar{Q}^{g,0}_{i,j,m} + \frac{2\sin\bar{\theta}_j}{\Delta z}\psi^{g,-}_{i,j,k}(s) \quad (8)$$

The term $\frac{2\sin\bar{\theta}_j}{\Delta z}\psi^{g,-}_{i,j,k}(s)$ on the right-side act as a surface source from the bottom plane. It merged with the fission and scattering source.

$$\frac{2\sin\bar{\theta}_j}{\Delta z}\psi^{g,-}_{i,j,k}(s) \approx \frac{2\sin\bar{\theta}_j}{\Delta z}\bar{\bar{\psi}}^{g,-}_{i,j}(s)$$

where, $\bar{\bar{\psi}}^{g,-}_{i,j}(s)$ is region average angular flux.

Finally, the general form of transport equation is

$$cos\,\bar{\theta}_j \frac{\partial \psi^{g,0}_{i,j,k}(s)}{\partial s} + \tilde{\Sigma}^g_{tr,m}\psi^{g,0}_{i,j,k}(s) = \bar{S}^{g,0}_{i,j,m} \quad (9)$$

where, $\tilde{\Sigma}^g_{tr,m}$is the modified transport cross section is defined as,

$$\tilde{\Sigma}^g_{tr,m} = \frac{2\sin\bar{\theta}_j}{\Delta z} + \Sigma^g_{tr,m}$$

and, the total source is defined as

$$\bar{S}^{g,0}_{i,j,m} = \bar{Q}^{g,0}_{i,j,m} + \frac{2\sin\bar{\theta}_j}{\Delta z}\psi^{g,-}_{i,j,k}(s)$$

The analytical solution of Eq. (9) is

$$\psi^{g,0}_{out,i,j,k} = \psi^{g,0}_{in,i,j,k}e^{-\tilde{\Sigma}^g_{tr,m}t'_{i,j,k}} + \frac{\bar{S}^g_{i,j,m}}{\tilde{\Sigma}^g_{tr,m}}\left(1 - e^{-\tilde{\Sigma}^g_{tr,m}t'_{i,j,k}}\right) \quad (10)$$

where $\psi^{g,0}_{out,i,j,k}$ is the outgoing angular flux from the ray segment; $\psi^{g,0}_{in,i,j,k}$is the incoming angular flux to the segment; $t_{i,j,k}$ the length of the segment projected on x-y plane; ; $t'_{i,j,k}$is the actual length of segment.

The track average angular flux is defined as,

$$\bar{\psi}^{g,0}_{i,j,k} = \frac{\int_0^{t'_{i,j,k}}\psi^{g,0}_{i,j,k}(s)ds}{\int_0^{t'_{i,j,k}}ds} = \frac{\int_0^{t'_{i,j,k}}\{\psi^{g,0}_{i,j,k}(0)e^{-\tilde{\Sigma}^g_{tr,m}s} + \frac{\bar{S}^g_{i,j,m}}{\tilde{\Sigma}^g_{tr,m}}\left(1 - e^{-\tilde{\Sigma}^g_{tr,m}s}\right)\}ds}{t'_{i,j,k}}$$

$$= \frac{\bar{S}^g_{i,j,m}}{\Sigma^g_{tr,m}} + \frac{1}{\tilde{\Sigma}^g_{tr,m}t'_{i,j,k}}(\psi^{g,0}_{in,\,i,j,k} - \frac{\bar{S}^g_{i,j,m}}{\Sigma^g_{tr,m}})(1 - e^{-\tilde{\Sigma}^g_{tr,m}t'_{i,j,k}}) \quad (11)$$

The region average angular flux is defined as,

$$\bar{\bar{\psi}}^{g,0}_{i,j,m} = \frac{\sum_{k\in m}\bar{\psi}^{g,0}_{i,j,k}t'_{i,j,k}d_i}{\sum_{k\in m}t'_{i,j,k}d_i} = \sum_{k\epsilon m}[\frac{\bar{S}^g_{i,j,m}}{\Sigma^g_{tr,m}} + \frac{d_i\,cos\,\theta_j}{\tilde{\Sigma}^g_{tr,m}A_m}\left(\frac{\bar{S}^g_{i,j,m}}{\Sigma^g_{tr,m}} - \psi^{g,0}_{in,\,i,j,k}\right)\left(1 - e^{-\tilde{\Sigma}^g_{tr,m}t'_{i,j,k}}\right)] \quad (12)$$

where d_i is the ray spacing and A_m is the analytic area of flat source region m.

The flat source region-wise scalar flux is calculated as

$$\phi^{g,0}_m = 4\pi\sum_j\sum_i\bar{\bar{\psi}}^{g,0}_{i,j,m}\omega_i\omega_j \quad (13)$$

where ω_i and ω_j are the weights for the azimuthal angle and polar angle, respectively.

2.2 MOC Scattering Source

The angular dependence of the scattering cross section is expanded into a series of Legendre polynomials [2]. The scattering source is a function of incoming and outgoing direction of flight or the cosine of the angle between them and can be expanded in terms of scattering angle:

$$\sigma_s(r, E'\to E, \mu_0) = \frac{1}{4\pi}\sum_{l=0}^{N}(2l+1)\,\sigma^l_s(r,E')P_l(\mu_0) \quad (14)$$

Apply the spherical harmonic theorem into Eq. (14)

$$P_l(\mu_0) = \frac{4\pi}{2l+1}\sum_{m=-l}^{l}Y_{l,m}(\Omega) \quad (15)$$

From Eq. (7), the total source is the sum of fission and scattering source. The scattering source term is defined by

$$Q_s(r,E,\Omega) = \int_0^\infty dE'\int_0^{4\pi}d\Omega'[\sigma_s(r,E'\to E,\Omega'.\Omega)\psi(r,E',\Omega')] \quad (16)$$

The spherical harmonics functions $Y_{l,m}(\Omega)$in Eq. 15 is defined by:

$$Y_{l,m}(\Omega) = \sqrt{\frac{(2l+1)}{4\pi}}\sqrt{\frac{(l-|m|)!}{(l+|m|)!}}P_{l,|m|}(\mu)e^{im\varphi}\ ,0 \le |m| \le n \le \infty \quad (17)$$

$P_{l,m}(\mu)$is the associate Legendre function and μ and φ are the cosine of polar angle and azimuthal angle of the direction of vector Ω.

$$P_{l,m}(\mu) = \begin{cases} (-1)^m(1-\mu^2)^{\frac{m}{2}}\left(\frac{d}{d\mu}\right)^m P_l(\mu) & m \ge 0 \\ (-1)^m\left(\frac{(l-|m|)!)}{(l+|m|)!}\right)P_{l,|m|}(\mu) & m < 0 \end{cases}$$

The scattering source term change by replacing Eq. (16)

$$Q_s(r,E,\Omega) = \int_0^\infty dE'[\sum_{l=0}^{l}\sigma^l{}_s(r,E'\to E)\sum_{m=-l}^{l}\psi_{l.m}(r,E')Y_{l,m}(\Omega)]$$

$$Q_s(r,E,\Omega) = \int_0^\infty dE'[\sum_{l=0}^{l}\sigma^l{}_s(r,E'\to E)\{\psi_{l.0}(r,E')Y_{l,0}(\Omega) + \sum_{m=1}^{l}(\psi_{l.m}(r,E')Y_{l,m}(\Omega) + \psi^*{}_{l.m}(r,E')Y^*{}_{l.m}(\Omega))\}]$$

By putting real and imaginary part of each component then we can write,

$$Q_s(r,E,\Omega) = \int_0^\infty dE'[\sum_{l=0}^{l}\sigma^l{}_s(r,E'\to E)\{\psi_{l.0}(r,E')Y_{l,0}(\Omega) + 2\sum_{m=1}^{l}(\psi_{l.m(Re)}(r,E')Y_{l,m(Re)}(\Omega) + \psi_{l.m(Im)}(r,E')Y_{l.m(Im)}(\Omega))\}]$$

More simplified,

$$Q_s(r,E,\Omega) = \int_0^\infty dE'[\sum_{l=0}^{l}\sigma^l{}_s(r,E'\to E)\sum_{m=-l}^{l}R_{l,m}(\Omega)\psi_{l.m}(r,E')] \quad (18)$$

where,

$$R_{l,m}(\Omega) = \begin{cases} \sqrt{\frac{(2l+1)}{4\pi}}\sqrt{2\frac{(l-m)!}{(l+m)!}}P_{l,m}(\mu)\,cos(m\varphi) & m > 0 \\ \sqrt{\frac{(2l+1)}{4\pi}}P_l(\mu) & m = 0 \\ \sqrt{\frac{(2l+1)}{4\pi}}\sqrt{2\frac{(l-|m|)!}{(l+|m|)!}}P_{l,|m|}(\mu)\,sin(|m|\varphi) & m < 0 \end{cases}$$

and the angular flux (PN flux) moment are defined by

$$\phi^m_l(r,E') = \int_0^{4\pi}d\Omega' R_{l,m}(\Omega')\psi(r,E',\Omega') \quad (19)$$

where $R_{l,m}(\Omega')$ are the parts of the spherical harmonics.

3. Numerical Results

2D and 3D problem results will discuss at this section. All the analyses were done with MOC ray spacing 0.02 cm, azimuthal angles 96, with 6 polar angles. In 3D problem, black boundary is used at top and bottom and all other cases reflective boundary is used. The mesh for each pin cell consists of 5 radial rings for the inner zone, 3 radial rings for the outer zone and the axial mesh for the 3-D configuration consists of 144 plane (2.85 cm for fuel and 2.67 cm for reflector) as shown in Fig. 3.

3.1 Single Assembly

Pressurized water reactor fuel assembly (Westinghouse and OPR-1000 designed) were selected to demonstrate performance of higher order scattering source consideration. The Westinghouse-designed (WH) assembly consist of 17x17 matrix fuel array with 264 number of fuel rods, 24 guide and one instrument tubes as shown in Fig. 1(a). Fuel pin and assembly technical specification and reference solutions were taken from VERA core physics benchmark progression problem [3]. However, the assembly inter-gap is omitted. On the other hand, OPR-1000 assembly have 16x16 matrix with 236 number of fuel rods, 4 guide thimbles and one instrument tube as shown in Fig. 1(b). Both FA's have identical material compositions for fuel, cladding and moderator, i.e., 3.1 wt% UO2 fuel, 0.743 g/cc moderator with 1300 ppm of boron, and Zircaloy-4 cladding. The two FAs are at 600 K for all regions.

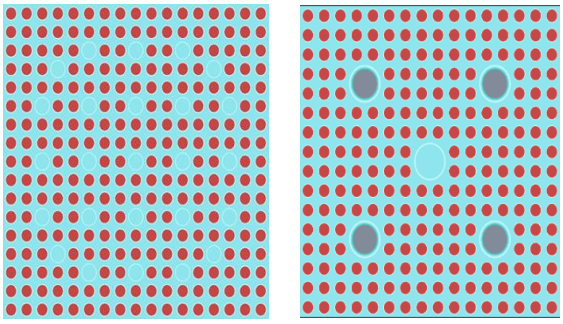

(a) (b)

Fig 1: Fuel Assembly (a) Westinghouse designed (unrodded) and (b) OPR-1000 designed (rodded).

Table 1 show the results of the unrodded and rodded FAs analyses. In the results, P3 and transport corrected P0 shows a similar level of accuracy in the rodded and unrodded analyses. On the other hand, P0 eigenvalue difference about 250 pcm in unrodded and more than 2000 pcm in rodded case. Overall eigenvalue difference within 50 pcm in both rodded and unrodded case at order 3 and below 0.5 percent maximum relative power.

3.2 B&W Simple Experiments

The Babcock & Wilcox (B&W) [5] Series 1484 core I and II experiments consist of two very simple cores (one circular and one square), as shown in Fig. 2. These cores contain no heterogeneities (e.g., water holes, absorber holes, enrichment splits), and since the cores differ in size and shape, they present a wide range of radial leakage core I consists of 458 identical fuel pins (2.459 wt%) arranged in a circular shape, which has been symmetrized for our purposes. This core is in a very high-leakage configuration. Core II consists of 1764 identical fuel pins (2.459 wt%) arranged in a square shape. This core is in a relatively low-leakage configuration. The two cores together core I and core II provide a very good indication of the accuracy with which radial leakage and anisotropic scattering.

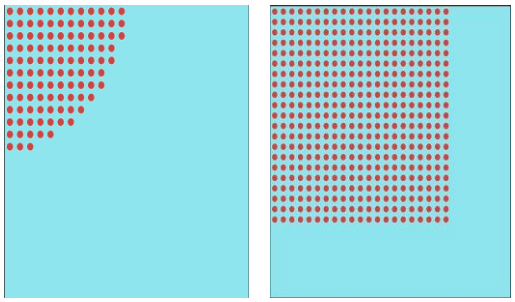

(a) (b)

Fig. 2: B&W Series 1484 (simple critical): (a) core I and (b) core II.

Tables 2 & 3 show the results of B&W series 1484 core I & II. Core I & II shows more than 11000 pcm and 5000 pcm difference at P0. On the other hand, k-effective compensate from 11000 pcm to 16 pcm and 5000 to 145 pcm at order P3. Maximum relative pin power differences were 1.5% and 0.99% at core I and II respectively and average percent RMS error were 0.49 and 0.18 respectively. However, maximum relative error increase from 1.5% to 10.73% and 0.99% to 22.78% at P0.

3.3 3D Single Assembly

In 3D case, similar specification fuel assembly was used which was used in section 3.1. the total height of the assembly was 407.84 cm included one assembly height 21.42 cm top and bottom water reflector as shown in Fig. 3. Black boundary condition is used at top and bottom and reflective all other sides. Only unrodded problems were analyses.

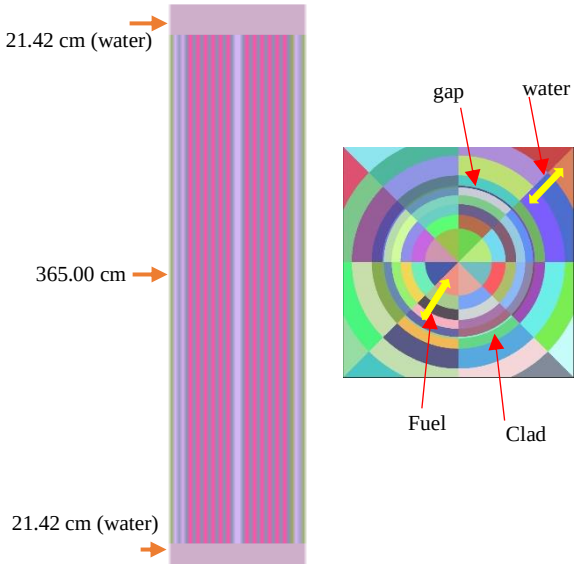

Fig 3: 3D Fuel Assembly and radial mesh (single pin).

Table 4 demonstrate the 3D single assembly results. The k-effective difference in both P0 and P3 are similar but in term of pin power difference P0 results is far away from reference. However, in P3, maximum relative pin power differences are 0.14% and -0.24% at WH and OPR-1000 design assembly respectively.

Table 1: Fuel assembly results

PN order	k-effective	diff.[a] (pcm)	Pin Power diff.[b]	
			PW.(%)	Max.(%)
WH (unrodded)				
Ref.[c]	1.18035	±3[d]	±0.04[d]	±0.06[d]
P3	1.18006	-29	0.16	0.45
P1	1.17940	-95	1.92	3.32
P0	1.17814	-221	2.76	4.85
P0_tr[e]	1.18047	12	0.07	0.19
WH (rodded)				
Ref.	0.78395	±3	±0.05	±0.06
P3	0.78425	-30	0.10	0.22
P1	0.78121	-273	1.01	3.19
P0	0.80548	-2153	2.76	5.10
P0_tr	0.78495	100	0.68	1.40
OPR-1000 (unrodded)				
Ref.	1.17471	±3	±0.04	±0.05
P3	1.17456	-15	0.12	-0.29
P1	1.17443	-28	0.16	-0.38
P0	1.17103	-368	0.76	1.77
P0_tr	1.17439	-32	0.09	-0.20
OPR-1000 (rodded)				
Ref.	0.94874	±3	±0.05	±0.05
P3	0.94823	-51	0.15	-0.42
P1	0.94607	-267	0.17	-0.50
P0	0.97182	2307	1.22	2.21
P0_tr	0.95042	167	0.15	-0.34

[a] difference = $(k_{eff} - k_{eff}^{ref.})x10^{05}$
[b] difference of pin power: PW.: power weight difference; Max.: the maximum difference.
[c] Monte Carlo code MCS [4]
[d] RMS and the maximum pin power statistical errors of MCS results.
[e] P0_tr: transport corrected P0

Table 2: Summary results of 2D B&W 1484 core I

PN order	k-effective	diff.[b] (pcm)	Pin Power diff.[c]	
			PW.(%)	Max.(%)
Ref.	1.01560	±3	±0.03	±0.05
P3	1.01576	16	0.49	1.50
P1	1.01516	-44	1.65	2.91
P0	1.11986	10426	3.87	10.73
P0_tr	1.01713	153	0.71	1.23

Table 3: Summary results of 2D B&W 1484 core II

PN order	k-effective	diff.[b] (pcm)	Pin Power diff.[c]	
			PW.(%)	Max.(%)
Ref.	1.01592	±3	±0.09	±0.19
P3	1.01714	122	0.16	0.99
P1	1.01876	284	0.60	4.02
P0	1.05776	4184	3.20	22.78
P0_tr	1.01582	-10	0.33	1.75

Table 4: Summary results of 3D fuel assembly

PN order	k-effective	diff.[b] (pcm)	Pin Power diff.[c]	
			PW.(%)	Max.(%)
WH (unrodded)				
Ref.	1.17589	±3	±0.05	±0.06
P3	1.17672	83	0.09	0.14
P1	1.17719	130	0.14	0.21
P0	1.17731	142	0.36	0.89
P0_tr	1.17558	-31	0.14	0.23
OPR-1000 (unrodded)				
Ref.	1.17030	±3	±0.04	±0.05
P3	1.18006	94	0.10	-0.24
P1	1.17221	191	0.12	-0.34
P0	1.16838	-192	0.74	1.66
P0_tr	1.16978	-52	0.09	0.23

3. Conclusions

This paper has presented a general description of the PN theory behind the STREAM lattice physics code. A significant portion of the paper has been devoted to describing the way in which the MOC has been applied in STREAM. Calculations were performed with the ENDF/B-VII.1 data library and demonstrate excellent agreement with no obvious significant bias versus control rods and geometry. Although validation was done up to PN order 3. Significant k-effective differences were found between P0 and P3 except 3D single assembly case. But pin power distribution has a good agreement at P3. Finally, it is proved that using higher order might generate better accurate results.

4. Acknowledgement

This work was supported by the National Research Foundation of Korea (NRF) grant funded by the Korea government (MSIT). (No. NRF-2019R1C1C1010063).

REFERENCES

[1] Sooyoung Choi, Deokjung Lee, "Three-dimensional method of characteristics/diamond-difference transport analysis method in STREAM for whole-core neutron transport calculation", Computer Physics Communications, 28 April 2020, 107332.
[2] G. Palmiotti, E. E. Lewis , and C. B. Carrico, VARIANT: VARIational Anisotropic Nodal Transport for Multidimensional Cartesian and Hexagonal Geometry Calculation, ANL-95/40, Argonne National Laboratory, USA.
[3] A. T. Godfrey, Vera core physics benchmark progression problem specifications, Revision 4, CASL-U-2012-0131-004, CASL, 2014.
[4] Hyunsuk Lee, Wonkyeong Kim, Peng Zhang, Azamat Khassenov, Yunki Jo, Jinsu Park, Jiankai Yu, Matthieu Lemaire, Deokjung Lee*, "MCS – A Monte Carlo Particle Transport Code for Large-Scale Power Reactor Analysis," Annals of Nuclear Energy, 139: 107276.
[5] M. N. Baldwin, G. S. Hoovler, R. L. Eng, F. G. Welfare, Critical experiments supporting close proximity water storage of power reactor fuel, The Babcock & Wilcox Company, 1979.